

Photonics-based de-chirp processor with the capability of processing dual-band signals

Jiang Liu, Dan Zhu, Wenjuan Chen, and Shilong Pan
Nanjing University of Aeronautics and Astronautics, Nanjing, People's Republic of China

Email: danzhu@nuaa.edu.cn

A photonics-based de-chirp processor with the capability of processing dual-band linearly frequency-modulated (LFM) waveforms is proposed and demonstrated. Two de-chirped signals will be output simultaneously and independently, while no special requirement of the input signals' chirp rates is needed. A proof-of-concept experiment is carried out. De-chirp processing of dual-band signals (X- and Ku-band) is successfully implemented. The crosstalk suppression ratio of more than 40 dB is achieved with de-chirped results in the two bands.

Introduction: In order to achieve the cognition ability to learn, infer and react to the environment, multiple functions working in different optimal frequency bands are required with the future radar systems [1–4]. The limitations in the working frequency and bandwidth bring a great challenge to the electronic technologies. Microwave photonics is enabling new paradigms for multi-band applications since photonics can introduce the advantages of large working bandwidth, parallel processing, and so on.

The linearly frequency-modulated (LFM) signals are typical radar signals, with which the de-chirp processing is a typical pulse compression method. The key challenge for dual-band processing is how to avoid the interference with each other of the obtained information from different bands [5, 6]. Photonics-based dual-band de-chirp processing schemes have been verified in [5, 6]. In [5], by using a dual-polarisation quadrature phase shift keying (DP-QPSK) modulator, the 1st order optical sidebands are generated by modulating the reference and the echo signals of one band at the sub-MZMs with the peak biasing points, while the 2nd order optical sidebands are generated by modulating those of the other band at the sub-MZMs with the null biasing points. After the optical to electrical conversion, the dual-band signals are successfully de-chirped. However, the chirp rates of the two-band signals and the movement range of the detected target must satisfy a specific requirement. In [6], by introducing a photonics-based I/Q mixer, the de-chirped results of the signals in two bands are obtained and located in the positive and negative spectrum, respectively. However, the dual-band LFM signals need to be specially designed with inverse chirp rates.

Here, a photonics-based dual-band de-chirp processor is proposed and demonstrated. Two de-chirped results with the dual-band signals will be output simultaneously and independently, while no special requirement with the input signals' chirp rates is needed. A proof-of-concept experiment is carried out. The de-chirp processing with the dual-band signals (X- and Ku-band) is successfully achieved, with the crosstalk suppression ratio being more than 40 dB.

Principle: The scheme of the proposed photonics-based dual-band de-chirp processor is shown in Figure 1. The optical carrier is split into two parts and injected into two dual parallel Mach-Zehnder modulators (DPMZMs), respectively. The reference signals of the two bands are modulated to DPMZM1 through one controllable phase shifter network, while the echo signals are modulated to DPMZM2 through the other one. The optical outputs from the two DPMZMs are injected into the optical LO and signal ports of a 90° optical hybrid, respectively. The 90° optical hybrid is followed by two balanced photodetectors (BPDs) and a 90° electrical hybrid. The de-chirped results with the two-band echoes will be output from the two output ports of the 90° electrical hybrid, respectively. As compared with [6], by introducing the controllable phase shifter network, the de-chirp processing of the dual-band signals with independent chirp rates is achieved.

The structure of the controllable phase shifter network is shown in detail in the inset of Figure 1a, which can be achieved through us-

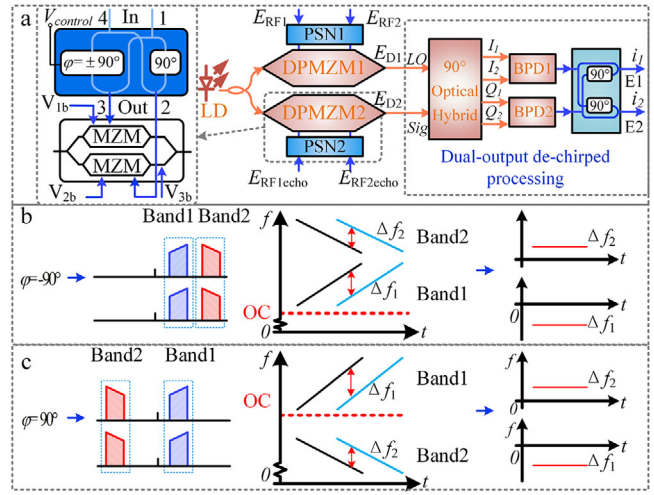


Fig. 1 (a) The schematic diagram of the photonics-based dual-band de-chirp processor. LD: laser diode, DPMZM: dual-parallel Mach-Zehnder modulator, PSN: phase shifter network, BPD: balanced photodetector. (Inset: The structure of the controllable PSN and the connection with the DPMZM). The working principle when the processed dual-band signals have (b) inverse chirp rates, (c) both positive (or negative) chirp rates. OC: optical carrier

ing the techniques in [7]. The transform matrix of the network is as follows

$$S = \begin{bmatrix} S_{11} & S_{12} & S_{13} & S_{14} \\ S_{21} & S_{22} & S_{23} & S_{24} \\ S_{31} & S_{32} & S_{33} & S_{34} \\ S_{41} & S_{42} & S_{43} & S_{44} \end{bmatrix} = \frac{-1}{\sqrt{2}} \begin{bmatrix} 0 & j & 1 & 0 \\ j & 0 & 0 & 1 \\ 1 & 0 & 0 & \varphi \\ 0 & 1 & \varphi & 0 \end{bmatrix} \quad (1)$$

By injecting the two-band reference signals of E_{RF1} and E_{RF2} into port 1 and port 4, respectively, the outputs from port 2 and port 3 are as follows

$$\begin{bmatrix} E_2 \\ E_3 \end{bmatrix} = \begin{bmatrix} E_{RF1} \\ E_{RF2} \end{bmatrix} \begin{bmatrix} S_{21} & S_{24} \\ S_{31} & S_{34} \end{bmatrix} = \begin{bmatrix} E_{RF1} \angle 90^\circ + E_{RF2} \\ E_{RF1} + E_{RF2} \angle \varphi \end{bmatrix} \quad (2)$$

Then E_2 and E_3 are sent to the two RF ports of DPMZM1, respectively. The optical signal injected into DPMZM1 is $E_{in} = E_0 \exp(j\omega_0 t)$. E_{RF1} has the frequency of ω_{RF1} , while E_{RF2} has the frequency of ω_{RF2} . Considering the small signal modulation case, only the optical carrier and the ± 1 -order optical sidebands are considered. The optical output from DPMZM1 is

$$\begin{aligned} E(t) &= \frac{1}{2} E_0 e^{j\omega_0 t} \{ [e^{j\beta E_2} + e^{j\Delta\theta_2} e^{-j\beta E_3}] e^{j\Delta\theta_1} + (e^{j\beta E_2} + e^{j\theta_3} e^{-j\beta E_3}) \} \\ &= \frac{1}{2} E_0 \{ [e^{j\Delta\theta_1} (1 + e^{j\Delta\theta_2}) + 1 + e^{j\Delta\theta_3}] J_0(\beta) \\ &\quad + [e^{j\Delta\theta_1} - e^{j(\Delta\theta_1 + \Delta\theta_2)} + e^{-j\pi/2} - e^{(\Delta\theta_3 - \pi/2)}] J_{-1}(\beta) e^{j(\omega_0 - \omega_{RF1})t} \\ &\quad + [e^{j\Delta\theta_1} - e^{j(\Delta\theta_1 + \Delta\theta_2)} + e^{j\pi/2} - e^{(\Delta\theta_3 - \pi/2)}] J_1(\beta) e^{j(\omega_0 + \omega_{RF1})t} \\ &\quad + [e^{j\Delta\theta_1} - e^{j(\Delta\theta_1 + \Delta\theta_2)} + e^{-j\pi/2} - e^{(\Delta\theta_3 + \varphi)}] J_{-1}(\beta) e^{j(\omega_0 - \omega_{RF2})t} \\ &\quad + [e^{j\Delta\theta_1} - e^{j(\Delta\theta_1 + \Delta\theta_2)} + e^{j\varphi} - e^{(\Delta\theta_3 - \varphi)}] J_1(\beta) e^{j(\omega_0 + \omega_{RF2})t} \} \quad (3) \end{aligned}$$

where β denotes the modulation index, $\Delta\theta_1$, $\Delta\theta_2$ and $\Delta\theta_3$ are the phase differences introduced by the DC biases of V_{1b} , V_{2b} and V_{3b} applied to DPMZM1, respectively, and $J_{\pm 1}(\cdot)$ is the ± 1 -order Bessel function of the first kind. When $\Delta\theta_1 = 90^\circ$, $\Delta\theta_2 = \Delta\theta_3 = 180^\circ$, only the +1st-order optical sideband corresponding to E_{RF1} is remained. By setting $\varphi = -90^\circ$, only the +1st-order optical sideband corresponding to E_{RF2} is remained. By setting $\varphi = 90^\circ$, only the -1st-order optical sideband corresponding to E_{RF2} is remained.

In this way, when modulating the reference and the echo signals of an LFM signal with the expression of $\cos(\omega_R t + k\pi t^2)$ (here ω_R and k are

the initial frequency and the chirp rate, respectively) to DPMZM1 and DPMZM2, respectively, the optical outputs from the two modulators are

$$\begin{cases} E_{D1} = E_0 J_1(\beta) \exp[j(\omega_0 t + \omega_R t + k\pi t^2)] \\ E_{D2} = E_0 J_1(\beta) \exp[j(\omega_0(t - \tau) + \omega_R(t - \tau) + k\pi(t - \tau)^2)] \end{cases} \quad (4)$$

where τ denotes the time delay between the echo and the reference signals. The two optical outputs are sent to the optical LO and RF ports of a 90° optical hybrid, respectively. Two in-phase outputs ($I_1 \propto E_{D2} + E_{D1}$, $I_2 \propto E_{D2} - E_{D1}$) and two quadrature outputs ($Q_1 \propto E_{D2} + jE_{D1}$, $Q_2 \propto E_{D2} - jE_{D1}$) will be output from the 90° optical hybrid, which are then injected into two BPDs, respectively. The outputs of the two BPDs can be expressed as

$$\begin{cases} i_{BPD1} = 2E_0 J_1(\beta) \{ \exp[j(\alpha + 2k\pi\tau t)] + \exp[-j(\alpha + 2k\pi\tau t)] \} \\ i_{BPD2} = 2E_0 J_1(\beta) \left\{ \exp\left[j\left(\alpha + 2k\pi\tau t + \frac{\pi}{2}\right)\right] + \exp\left[-j\left(\alpha + 2k\pi\tau t + \frac{\pi}{2}\right)\right] \right\} \end{cases} \quad (5)$$

where $\alpha = \omega_0\tau + \omega_R\tau - k\pi\tau^2$. The two signals are injected into the 90° electrical hybrid, with the outputs from port E1 and port E2 as follows

$$\begin{cases} i_1 \propto i_{BPD1} + i_{BPD2} \angle \frac{\pi}{2} \propto \begin{cases} 8E_0 J_1(\beta) \cos(\alpha + 2k\pi\tau t), & \text{when } k < 0 \\ 0, & \text{when } k > 0 \end{cases} \\ i_2 \propto i_{BPD1} \angle \frac{\pi}{2} + i_{BPD2} \propto \begin{cases} 0, & \text{when } k < 0 \\ 8E_0 J_1(\beta) \cos(\alpha + 2k\pi\tau t - \pi/2), & \text{when } k > 0 \end{cases} \end{cases} \quad (6)$$

It can be seen that the de-chirped result will be output from port E1 when the chirp rate is negative, and from port E2 when the chirp rate is positive.

When the dual-band signals have inverse chirp rates, containing the RF signals of $E_{RF1} = \cos(\omega_1 t + k_1 \pi t^2)$ and $E_{RF2} = \cos(\omega_2 t - k_2 \pi t^2)$, the working principle is shown in Figure 1b. The value of φ in the phase shifter networks is set to be -90° , and the chirp rate symbols of the two optically carried LFM signals are opposite. Thus the de-chirped results corresponding to the two bands ($\Delta f_1 = -k_1 \tau_1$ and $\Delta f_2 = k_2 \tau_2$) will output from the two ports of the 90° electrical hybrid, respectively.

In the other condition, the dual-band signals have positive (or negative) chirp rates. Take the condition with the positive chirp rates as an example, i. e., $E_{RF1} = \cos(\omega_1 t + k_1 \pi t^2)$, $E_{RF2} = \cos(\omega_2 t + k_2 \pi t^2)$. As shown in Figure 1c, the value of φ is set to be 90° , and the -1^{st} -order sideband of the optically carried RF signal of E_{RF2} will remain. In this way, the chirp rate symbols of the optically carried LFM signals in the two bands are also opposite. Thus the corresponding de-chirped results ($\Delta f_1 = -k_1 \tau_1$ and $\Delta f_2 = k_2 \tau_2$) will also output from the two ports of the 90° electrical hybrid, respectively.

Experiment: A proof of the concept experiment is demonstrated based on the scheme shown in Figure 1a. A CW light at 1550.53 nm with a power of 16 dBm is generated from a laser diode (LD, Teraxion Inc., NLL). Two DPMZMs (Fujitsu, FTM7961EX, 35 Gbps) with the half-wave voltage of 3.5 V are used. The dual-band LFM waveforms are generated by an arbitrary waveform generator (AWG, Keysight M8195A, 65 GSa/s). Limited by the experimental condition, the controllable phase shifter network is realised by two adjustable phase shifters (Natick, MODEL 6705K-2, DC-26.5 GHz), one of which realises the 90° phase difference between the outputs from port 2 and port 3 when the signal is input from port 1, and the other one realises the adjustment of the $\pm 90^\circ$ phase difference between the outputs from port 2 and port 3 when the signal is input from port 4. A 90° optical hybrid (Kylia COH24) with a phase accuracy of 1.5° is used. Two BPDs (BPDV2150R-VF-FP, 0.53-A/W responsivity) with 40 GHz working bandwidth are used. The electrical signals are sampled by an oscilloscope (Agilent, DSO-X 92504A, 80 GSa/s). The optical spectra are obtained by an optical spectrum analyzer (APEX AP2040d) with the resolution set to be 20 pm.

Firstly, the de-chirp processing with the dual-band signals having inverse chirp rates is experimentally investigated. The dual-band LFM waveforms include an X-band LFM signal with a positive chirp rate of 10^5 GHz/s and a Ku-band LFM signal with a negative chirp rate of -8×10^4 GHz/s. The initial frequency and bandwidth of the X-band signal are 9.5 and 1 GHz, respectively, while those of the Ku-band signal are 16.4 and 0.8 GHz, respectively. The time delay between the echo signals and the reference signals is introduced by a single-mode fibre. Figures 2a and 2b show the optical spectra at the outputs of DPMZM1 and DPMZM2,

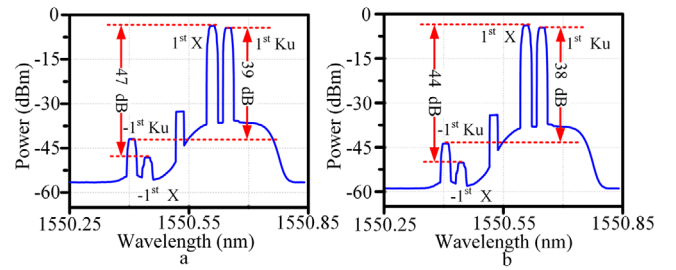


Fig. 2 The experimentally obtained optical spectra at the outputs of (a) DPMZM1 driven by the reference signals, (b) DPMZM2 driven by the echo signals, when the dual-band signals have inverse chirp rates

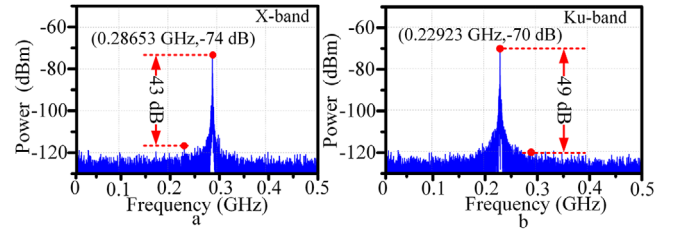


Fig. 3 The experimentally obtained electrical spectra of the de-chirped results of the (a) X-, (b) Ku-band signals with inverse chirp rates

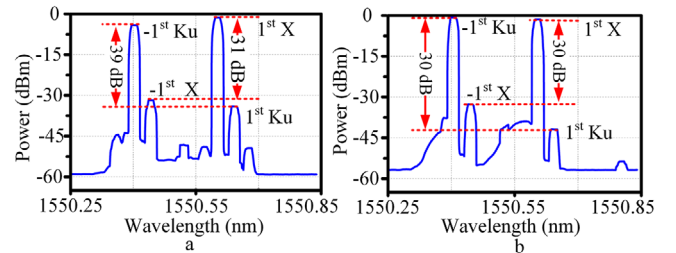


Fig. 4 The experimentally obtained optical spectra at the outputs of (a) DPMZM1 driven by the reference signals, (b) DPMZM2 driven by the echo signals, when the dual-band signals have both positive chirp rates

respectively. As can be seen, the sideband suppression ratios (SSRs) of the optically carried reference RF signals of E_{RF1} and E_{RF2} are 47 and 39 dB, respectively. The SSRs of the optically carried echo signals in the two bands are 44 and 38 dB, respectively. Due to the lack of low-frequency 90° electrical hybrid, the outputs from the BPDs are measured by the real-time oscilloscope, which are then processed in the digital domain to realise the function of a 90° electrical hybrid. The electrical spectra of the de-chirped results with the X- and Ku-band signals are shown in Figures 3a and 3b, respectively, which are located at 0.28653 and 0.22923 GHz, respectively. The crosstalk suppression ratios are 43 and 49 dB, respectively.

Then the chirp rates of the dual-band signals are both set to be positive, with the values of 10^5 and 8×10^4 GHz/s for X- and Ku-bands, respectively. The initial frequencies are 9.5 and 15.6 GHz for the two bands, respectively. The optical spectra output from DPMZM1 and DPMZM2 are shown in Figures 4a and 4b, respectively. The SSRs of the optically carried reference RF signals in the two bands are 31 and 39 dB, respectively. The SSRs of the optically carried echo signals of the two bands are both 30 dB. The electrical spectra of the de-chirped results with the X- and Ku-band echo signals are shown in Figure 5, which are located at 0.28653 and 0.22923 GHz, respectively. As can be seen, the crosstalk suppression ratio of 40 dB is achieved with the de-chirped results in the two bands.

Conclusion: A photonics-based de-chirp processor with the capability of processing dual-band LFM waveforms is proposed and demonstrated. Two de-chirped results with the dual-band signals can be simultaneously output without interfering with each other. No special requirement with the input signal's chirp rates is needed. A proof-of-concept experiment is carried out. The de-chirp processing with the dual-band signals (X- and

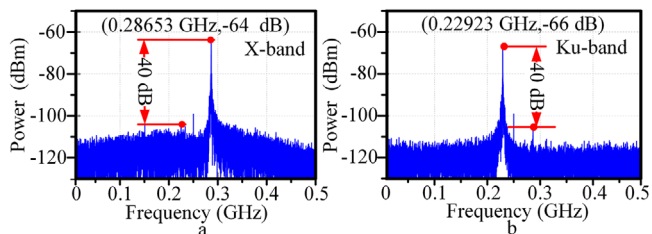


Fig. 5 The experimentally obtained electrical spectra of the de-chirped results of the (a) X-, (b) Ku-band signals with positive chirp rates

Ku-band) is successfully achieved, for both conditions when the dual-band signals have inverse or non-inverse chirp rates. The crosstalk suppression ratios of no less than 40 dB are successfully achieved. The proposed scheme can find applications in future multi-band radar systems.

Acknowledgement: This work was supported by the Fundamental Research Funds for Central Universities under Grant NE20170002.

© 2021 The Authors. *Electronics Letters* published by John Wiley & Sons Ltd on behalf of The Institution of Engineering and Technology

This is an open access article under the terms of the Creative Commons Attribution License, which permits use, distribution and reproduction in any medium, provided the original work is properly cited.

Received: 12 December 2020 Accepted: 23 March 2021

doi: 10.1049/ell2.12172

References

- 1 Munoz-Ferreras, J.-M., et al.: A deramping-based multiband Radar sensor concept with enhanced ISAR capabilities. *IEEE Sens. J.* **13**(9), 3361–3368 (2013)
- 2 Ghelfi, P., et al.: A fully photonics-based coherent radar system. *Nature* **507**(7492), 341–345 (2014)
- 3 Haykin, S.: Cognitive radar: A way of the future. *IEEE Signal Process. Mag.* **23**(1), 30–40 (2006)
- 4 Zhu, D., Pan, S.: Broadband cognitive radio enabled by photonics. *J. Lightwave Technol.* **38**(12), 3076–3088 (2020)
- 5 Cao, J., et al.: Photonics deramp receiver for dual-band LFM-CW radar. *J. Lightwave Technol.* **37**(10), 2403–2408 (2019)
- 6 Meng, Z., et al.: Dual-band dechirping LFMCW radar receiver with high image rejection using microwave photonic I/Q mixer. *Opt. Express* **25**(18), 22055–22065 (2017)
- 7 Anjos, E.V.P., et al.: Variable-phase all-pass network synthesis and its application to a 14–54 GHz multiband continuous-tune phase shifter in silicon. *IEEE Trans. Microwave Theory Tech.* **68**(8), 3480–3496 (2020)